Small Hepatocellular Carcinomas: Improved Sensitivity by Combining Gadoxetic Acid–enhanced and Diffusion-weighted MR Imaging Patterns[1]

Min Jung Park, MD, PhD
Young Kon Kim, MD, PhD
Min Woo Lee, MD, PhD
Won Jae Lee, MD, PhD
Young-Sun Kim, MD, PhD
Seong Hyun Kim, MD, PhD
Dongil Choi, MD, PhD
Hyunchul Rhim, MD, PhD

Purpose: To determine if the combination of gadoxetic acid–enhanced magnetic resonance (MR) imaging and diffusion-weighted (DW) imaging helps to increase accuracy and sensitivity in the diagnosis of small hepatocellular carcinomas (HCCs) compared with those achieved by using each MR imaging technique alone.

Materials and Methods: The institutional review board approved this retrospective study and waived the requirement for informed consent. The study included 130 patients (95 men, 35 women) with 179 surgically confirmed small HCCs (≤2.0 cm) and 130 patients with cirrhosis (90 men, 40 women) without HCC who underwent gadoxetic acid–enhanced MR imaging and DW imaging at 3.0 T between May 2009 and July 2010. Three sets of images were analyzed independently by three observers to detect HCC: a gadoxetic acid set (unenhanced, early dynamic, and hepatobiliary phases), a DW imaging set, and a combined set. Data were analyzed by using alternative-free response receiver operating characteristic analysis. Diagnostic accuracy (area under the receiver operating characteristic curve [A_z]), sensitivity, specificity, and positive predictive value were calculated.

Results: The mean A_z values for the combined set (0.952) were significantly higher than those for the gadoxetic acid set (A_z = 0.902) or the DW imaging set alone (A_z = 0.871) ($P \leq .008$). On a per-lesion basis, observers showed higher sensitivity in their analyses of the combined set (range, 91.1%–93.3% [163–167 of 179]) than in those of the gadoxetic acid set (range, 80.5%–82.1% [144–147 of 179]) or the DW imaging set alone (range, 77.7%–79.9% [139–143 of 179]) ($P \leq .003$). Positive predictive values and specificity for all observers were equivalent for the three imaging sets.

Conclusion: The combination of gadoxetic acid–enhanced MR imaging and DW imaging yielded better diagnostic accuracy and sensitivity in the detection of small HCCs than each MR imaging technique alone.

Supplemental material: *http://radiology.rsna.org/lookup/suppl/doi:10.1148/radiol.12112517/-/DC1*

[1] From the Department of Radiology and Center for Imaging Science, Samsung Medical Center, Sungkyunkwan University School of Medicine, 50 Irwon-dong, Gangnam-gu, Seoul 135-710, Republic of Korea. Received November 23, 2011; revision requested January 11, 2012; revision received February 3; accepted March 2; final version accepted March 22. **Address correspondence to** Y.K.K. (e-mail: *jmyr@dreamwiz.com*).

Hepatocellular carcinoma (HCC) is the most common primary liver cancer and is the third leading cause of cancer-related mortality worldwide (1). The presence of satellite nodules and vascular invasion are the most important negative prognostic factors (2,3). The importance of early detection of HCC has been emphasized, and the advances in curative therapies, including surgical and local-regional treatment, have contributed to the improved prognosis of patients with early-stage HCC (4,5).

Gadoxetic acid disodium, (Primovist [Eovist in the United States], Bayer-Schering, Berlin) is a magnetic resonance (MR) imaging contrast agent that has gained attention because it can provide, in a single examination, comprehensive hemodynamic information during early dynamic phases and improved lesion detection in the hepatobiliary phase (HBP) (6,7). HBP images better depict HCC, which appears as a hypointense lesion, compared with conventional dynamic gadolinium-enhanced images, on which small HCCs frequently (33.8%, 69 of 204 [8], 22.9%, 40 of 175 [9], 27%, 16 of 60 [10]) show only arterial enhancement without early washout (6,7).

Owing to its peculiar ability to allow differentiation of tissue on the basis of cellular density and architectural change in addition to vascularization, diffusion-weighted (DW) imaging has been applied increasingly to liver imaging (11–14). Because DW imaging is easy to perform and needs no contrast agent, it is routinely incorporated into standard clinical protocols. The evolution of HCC is a multifactorial process that includes cellular, architectural, and vascular changes. Accordingly, the addition of DW imaging to gadoxetic acid-enhanced MR imaging could be a promising strategy for both detection and characterization of HCC, due to its ability to target cellular and architectural changes through the differences in tissue diffusivity between HCC and benign hepatocellular nodules or parenchyma and hemodynamic changes. The authors of one recent study (15) reported that the combination of gadoxetic acid–enhanced MR imaging and DW imaging is helpful for the diagnosis of HCCs smaller than 1 cm. Therefore, we conducted this study to compare the diagnostic performance of combined gadoxetic acid–enhanced MR imaging and DW imaging with each type of imaging alone in the detection of HCCs 2 cm or smaller.

Advances in Knowledge

- The combination of gadoxetic acid–enhanced MR imaging and diffusion-weighted (DW) imaging yielded better sensitivity in the detection of small (≤2.0 cm) hepatocellular carcinomas (HCCs) than each MR imaging technique alone (combined, 92.4%; gadoxetic acid, 81.4%; DW, 78.8%; $P = .001$).
- The hyperintensity of solid masses on high-*b*-value DW imaging is highly indicative of HCC in patients with underlying chronic hepatitis or cirrhosis. The mean A_z values for the combination of gadoxetic acid-enhanced MR imaging and DW imaging ($A_z = 0.952$) were significantly higher than those for gadoxetic acid–enhanced imaging ($A_z = 0.902$) or DW imaging alone ($A_z = 0.871$) ($P \leq .008$).

Materials and Methods

Patient Selection

In this retrospective study, the sample size was determined on the basis of the primary hypothesis: that the difference in sensitivity with the use of the combination of gadoxetic acid–enhanced MR imaging and DW imaging and each MR procedure alone was 5%. Therefore, the appropriate sample size was 179 true-positive lesions, which ensured a power of 80% and a significance level of .05 (16).

Our study had institutional review board approval, and the requirement for informed consent was waived. We retrospectively reviewed our institutional database for liver MR imaging reports in patients suspected of having HCC who had undergone computed tomography (CT) at Samsung Medical Center, Sungkyunkwan University School of Medicine (Seoul, Korea), between May 2009 and July 2010. During this period, 2530 consecutively registered patients with chronic liver disease underwent liver MR imaging. MR examinations were performed to rule out or confirm HCC because of possible focal hepatic lesions found at ultrasonography or CT or elevated levels of serum tumor markers (α-fetoprotein or protein induced by vitamin K absence II). The inclusion criteria for the patient group were: *(a)* HCCs less than or equal to 2 cm in diameter that had been proved at surgical resection; *(b)* previous liver MR imaging with a 3.0 T system, including

Implication for Patient Care

- The addition of DW imaging to the routine protocol of gadoxetic acid–enhanced MR imaging may help to increase reader sensitivity in the detection of HCC and may be beneficial in the characterization of equivocal lesions.

Published online before print
10.1148/radiol.12112517 **Content code:** GI

Radiology 2012; 264:761–770

Abbreviations:

A_z = area under ROC curve
DW = diffusion weighted
HBP = hepatobiliary phase
HCC = hepatocellular carcinoma
ROC = receiver operating characteristic

Author contributions:

Guarantors of integrity of entire study, M.J.P., Y.K.K.; study concepts/study design or data acquisition or data analysis/interpretation, all authors; manuscript drafting or manuscript revision for important intellectual content, all authors; approval of final version of submitted manuscript, all authors; literature research, M.J.P., Y.S.K.; clinical studies, M.J.P., M.W.L., W.J.L., Y.S.K., S.H.K., D.C., H.R.; statistical analysis, M.J.P., Y.K.K.; and manuscript editing, M.J.P., Y.K.K., W.J.L., S.H.K., H.R.

Potential conflicts of interest are listed at the end of this article.

gadoxetic acid–enhanced imaging and DW imaging; and *(c)* no treatment for HCC before the MR examination. A total of 130 patients (95 men and 35 women; age range, 27–76 years) with 179 HCCs fit the inclusion criteria. We also selected 130 consecutive participants suspected of having HCC who had undergone liver MR imaging but had no identifiable HCCs to serve as a control group (Fig 1).

The characteristics for the patients and lesions are shown in Table 1. A total of 179 HCCs (mean size, 1.4 cm; range, 0.6–2.0 cm) were identified in the 130 patients, with lesions distributed as follows: patients with one lesion ($n = 99$), with two lesions ($n = 18$), with three lesions ($n = 9$), with four lesions ($n = 3$), and with five lesions ($n = 1$). Three dysplastic nodules identified at histopathologic analyses were also visible at MR imaging. In the 130 patients of the control group, 25 dysplastic nodules and three large regenerative nodules (mean size, 1.4 cm; range, 1.0–2.0 cm) were identified in 20 patients. Eosinophilic abscesses ($n = 7$), hemangiomas ($n = 22$), and nodular arterioportal shunts ($n = 84$) (mean size, 1.6 cm; range, 0.8–2.0 cm) were also identified among the HCC and control groups. Liver cirrhosis associated with hepatitis B virus was diagnosed in 242 patients, and the 18 remaining patients had hepatitis C virus–induced liver cirrhosis.

Figure 1

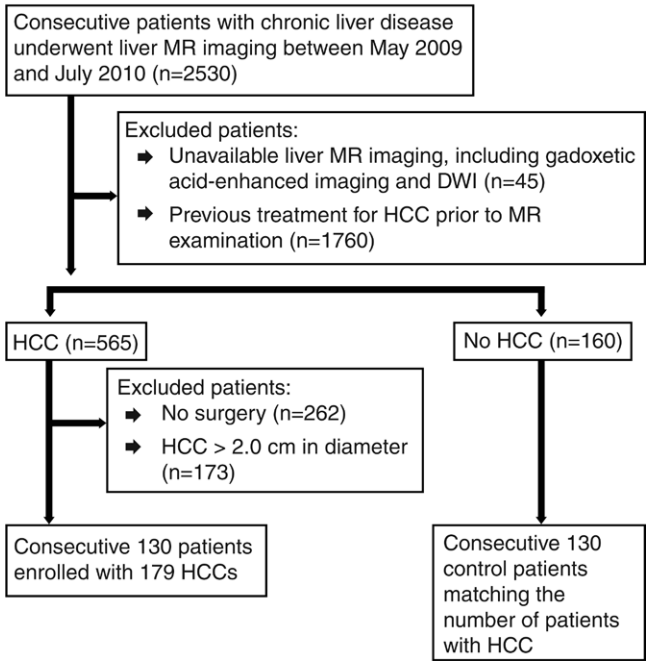

Figure 1: Flowchart of the study population.

Reference Standard

The reference standards for diagnosis of HCC, dysplastic nodules, regenerative nodules, and eosinophilic abscesses were based on the histopathologic examination of surgical specimens and sonographically guided percutaneous biopsy specimens. The average time interval between MR examination and surgery was 7 days (range, 3–12 days). The operations included segmentectomy ($n = 110$), bisegmentectomy ($n = 9$), lobectomy ($n = 13$), and liver transplantation ($n = 12$). Diagnoses of hemangiomas and arterioportal shunts were based on imaging findings and stability for at least 12 months of follow-up, except for one hyalinized hemangioma, which was diagnosed at histopathologic examination of the surgical specimen. The HCC patients and control patients underwent a series of follow-up CT and MR imaging examinations during the 10–16 months after the index MR imaging examination. In the follow-up studies, no additional HCCs were found.

MR Imaging

All MR images were acquired by using a 3.0-T whole-body MR system (Intera Achieva 3.0-T; Philips Healthcare, Best, the Netherlands) with a 16-channel phased-array coil that was used as the receiver coil. The baseline MR imaging included a T1-weighted turbo field echo in-phase and opposed-phase sequence, a breath-hold multishot T2-weighted sequence, and a respiratory-triggered heavily T2-weighted sequence (Table 2). DW images were acquired before the administration of gadoxetic acid by using a respiratory-triggered single-shot echo-planar imaging sequence with b values of 0, 100, and 800 sec/mm^2. A spectral attenuated inversion-recovery technique was used for fat suppression on DW images. The apparent diffusion coefficient was calculated by using a monoexponential function with b values of 100 and 800 sec/mm^2 to minimize perfusion effects.

For gadoxetic acid–enhanced imaging, unenhanced, arterial-phase (20–35 seconds), portal phase (60 seconds), late phase (3 minutes), and HBP (20 minutes) images were obtained by using a T1-weighted 3D turbo field-echo sequence (T1 high-resolution isotropic volume examination, eTHRIVE; Philips Healthcare) with a spectral attenuated inversion-recovery fat-suppression technique. The time for the arterial phase imaging was determined by using the MR fluoroscopic bolus detection technique. The contrast agent was administered intravenously by using a power injector at a rate of 1 mL/sec for a dose of 0.025 mmol per kilogram of body weight, followed by a 20-mL saline flush.

Image Analysis

All images were evaluated independently by three gastrointestinal radiologists: observer 1 (M.J.P., with 3 years of experience), observer 2 (M.W.L., with 7 years of experience), and observer 3 (Y.K.K.,

with 11 years of experience), who were blinded to whether the patients had HCC. The image review consisted of three reviewing sessions for three image sets, with a 2-week interval between image reviews. At the first reading session, the observers were randomly given either the gadoxetic acid set (unenhanced T1- and T2-weighted images and arterial, portal, 3 minute delay, and 20-minute HBP images) or the DW imaging set (unenhanced T1- and T2-weighted images and DW images) from the HCC and control groups. In the second session, observers received the image set they had not reviewed. Finally, the combined sets were reviewed. The order of case presentation was independently randomized in each session.

The observers assigned a confidence level to each diagnosis of a lesion on the basis of a four-point scale (1, probably not HCC; 2, possibly not HCC; 3, probably HCC; and 4, definitely HCC). MR images in which lesions were not detected were given a rating of 0. The diagnostic criteria for HCCs on the gadoxetic acid–enhanced images were a nodule showing enhancing foci during the arterial phase, washout during the portal venous phase or 3-minute delayed phase, and hypointensity during HBP. If a lesion was seen as hypointense only on HBP images or had nodules that showed enhancement only during the arterial phase, it was given a rating of 1 or 2, according to subjective judgment. On DW images, a lesion was considered to be HCC when it was hyperintense on b = 100 sec/mm^2 images, remained hyperintense on b = 800 sec/mm^2 images (Fig 2), and showed an apparent diffusion coefficient that was lower than or equal to that of the liver parenchyma (13). For the combined set, hypointense nodules without arterial hypervascularization on HBP images or nodules that showed only arterial enhancement and did not show hypointensity on HBP images but showed hyperintensity on DW images were also regarded as HCC. After the second review session, observer 1 and observer 3, in consensus, compared the scoring results of each observer with the reference standards and devised possible explanations for the causes of false-positive and false-negative results.

Table 1

Characteristics of Patients and Lesions

Characteristic	HCCs	Benign Lesions
Patient characteristic		
Age (y)	55.1 ± 7.9*	56.5 ± 8.6*
No. of men	95	90
No. of women	35	40
Child-Pugh class		
A	117	113
B	11	17
C	2	0
No. of lesions per patient	1–5 (1.4 ± 0.8)†	1–2 (1.1 ± 0.3)†
Lesion characteristic		
Category of lesion		
HCC grade 1	26	0
HCC grade 2	153	0
Dysplastic nodule	3	25
Regenerative nodule	0	3
Hemangioma	1	21
Eosinophilic abscess	1	6
Nodular arterioportal shunt	0	84
Diagnosed		
At operation	184 (HCC [n = 179], dysplastic nodule [n = 3], hemangioma [n = 1], eosinophilic abscess [n = 1])	17 (dysplastic nodule [n = 13], regenerative nodule [n = 2], Eosinophilic abscess [n = 2])
At percutaneous biopsy	0	17 (dysplastic nodule [n = 12], regenerative nodule [n = 1], eosinophilic abscess [n = 4])
At imaging follow-up	0	105 (arterioportal shunt [n = 84], hemangioma [n = 21])

* Data are mean ± standard deviation.

† Data are the range, with mean ± standard deviation in parentheses.

Statistical Analysis

Statistical analyses were performed by using statistical software (MedCalc version 11.4, MedCalc Software, Mariakerke, Belgium; SPSS version 18.0, SPSS, Chicago, Ill). Alternative-free-response receiver operating characteristic (ROC) curve analysis was performed on a lesion-by-lesion basis (17). The diagnostic accuracy of each set of images was assessed by calculating the area under the ROC curve (A_z), and the imaging sets for each observer were compared by using the variance z test. Considering the possible influence of lesion clustering on diagnostic accuracy, nonparametric analysis of clustered ROC curve data was performed by using the method proposed by Obuchowski (18). Among the 179 HCCs, the sensitivity for each set of images was evaluated according to the number of lesions with diagnoses that were assigned a confidence level of 3 or 4. The specificities and positive and negative predictive values of the sets of images were also calculated. Values of the sets of images were then compared by using the McNemar test. A P value less than .05 was considered to indicate a statistically significant difference. The κ statistic for multiple observers was calculated to assess the interobserver agreement (19). A κ value less than 0.20 indicated positive but poor agreement; 0.21–0.40, fair agreement; 0.41–0.60, moderate agreement; 0.61–0.80, good

Table 2

MR Imaging Sequences and Parameters

Sequence	TR/TE (msec)	Flip Angle (degrees)	Section thickness (mm)	Matrix Size	Bandwidth (Hz/pixel)	Acquisition Time (sec)	No of Signals Acquired
T1-weighted 2D dual gradient recalled echo	3.5/1.15–2.3	10	6	256 × 194	1918.6/0.226	14	1
Breath-hold multishot T2 weighted	1623/70	90	5	324 × 235	255.3/1.702	55/13.7	1
Breath-hold single-shot heavily T2 weighted	1156/160	90	5	376 × 270	388.9/1.117	120	2
DW imaging	1600/70	90	5	112 ×112	79.5/5.467	126	2
T1 weighted 3D gradient recalled echo	3.1/1.5	10	2	256 × 256	723.4/0.601	16.6	1

Note.—Field of view for all MR imaging sequences was 32–38 cm. TE = echo time, 3D = three-dimensional, TR = repetition time, 2D = two-dimensional.

Figure 2

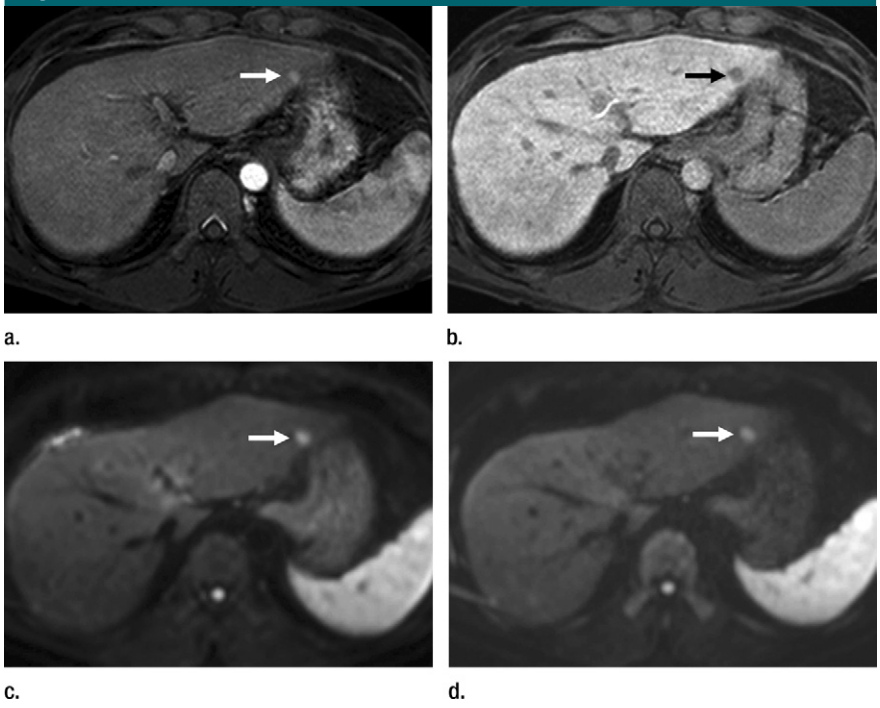

Figure 2: HCC in a 62-year-old man. Axial **(a)** arterial phase image and **(b)** HBP MR image obtained 20 minutes after administration of gadoxetic acid show small HCC with definitive arterial hypervascularization (arrow). HBP image (**b**) shows hypointensity (arrow). Single-shot echo-planar DW images at **(c)** $b = 100$ sec/mm^2 and **(d)** $b = 800$ sec/mm^2. Lesion shows clear hyperintensity (arrow). All observers diagnosed HCC with confidence levels of 3 or 4.

agreement; and greater than 0.81, excellent agreement.

Results

Of the 179 HCCs, 55 were 10 mm or less in diameter, and the remaining 124 were 11–20 mm in diameter. According to Edmondson's classification of HCC, 26 of 179 HCCs corresponded to criteria for grade 1, and the remaining 153 lesions were grade 2.

ROC Analysis

For all observers, nonparametric analysis of clustered ROC data showed that mean A_z values for the combined set for all HCCs and for HCCs 1 cm in diameter or smaller ($A_z = 0.952$ and $A_z = 0.911$, respectively), were significantly higher than those of the gadoxetic acid–enhanced set ($A_z = 0.902$, [$P < .001$] and $A_z = 0.773$ [$P < .001$], respectively) and the DW imaging set ($A_z = 0.871$ [$P < .001$] and $A_z = 0.738$ [$P < .001$]). (Table 3, Fig 2). For all observers, no significant difference was found between the gadoxetic acid set and the DW imaging set ($P > .05$).

Sensitivity and Specificity

The combined set yielded significantly higher mean sensitivity for all HCCs and for HCCs 1 cm or smaller (92.4% [496 of 537] and 84.8% [140 of 165], respectively) than did the gadoxetic acid set (81.4% [437 of 537] and 58.8% [97 of 165], respectively; $P < .001$) or the DW imaging set (78.8% [423 of 537] and 60.0% [99 of 165], respectively; $P = .003$). For HCCs larger than 1 cm, there was a significant difference in sensitivities between the combined set ($P = .003$) and the DW imaging set ($P = .006$). In the per-patient analysis, the combined set yielded significantly higher sensitivity (93.1% [121 of 130] for observer 1; 91.5% [119 of 130] for observer 2; and 93.8% [122 of 130] for observer 3) than did the gadoxetic acid set (82.3% [107 of 130] for observers 1 and 3; 83.9% [109 of 130] for observer 2) or the DW imaging set (79.2% [103 of 130] for all observers) ($P < .001$). There was no significant difference in sensitivities between the gadoxetic acid set and the DW imaging set ($P > .05$). For all observers, there were no significant differences

Table 3

A_z Values for the Detection of Small HCCs

	Observer 1		Observer 2		Observer 3		Pooled Data	
Imaging Modality	A_z Value	*P* Value	A_z Value	*P* Value	A_z Value	*P* Value	A_z Value	*P* Value
Gadoxetic acid set								
All lesions	0.906 ± 0.019	.003	0.894 ± 0.021	.004	0.904 ± 0.020	.008	0.902 ± 0.011	.001
≤ 1.0 cm	0.796 ± 0.049	.005	0.764 ± 0.053	.004	0.759 ± 0.052	.001	0.773 ± 0.009	.001
> 1.0 cm	0.957 ± 0.016	.771	0.952 ± 0.016	.877	0.971 ± 0.012	.948	0.960 ± 0.009	.318
DW imaging set								
All lesions	0.883 ± 0.021	.001	0.857 ± 0.023	.001	0.874 ± 0.022	.001	0.871 ± 0.013	.001
≤ 1.0 cm	0.766 ± 0.052	.001	0.694 ± 0.057	.001	0.754 ± 0.053	.001	0.738 ± 0.031	.001
> 1.0 cm	0.928 ± 0.020	.026	0.920 ± 0.021	.028	0.921 ± 0.021	.015	0.923 ± 0.012	.001
Combined set								
All lesions	0.958 ± 0.014	. . .	0.942 ± 0.016	. . .	0.956 ± 0.014	. . .	0.952 ± 0.009	. . .
≤ 1.0 cm	0.923 ± 0.031	. . .	0.889 ± 0.039	. . .	0.920 ± 0.031	. . .	0.911 ± 0.020	. . .
> 1.0 cm	0.972 ± 0.014	. . .	0.964 ± 0.015	. . .	0.971 ± 0.014	. . .	0.969 ± 0.009	. . .

Note.—Data are A_z values ± 1 standard deviation and *P* values comparing gadoxic acid and DW image sets with combined set.

Table 4

Sensitivity and Positive Predictive Values for the Detection of 179 HCCs

	Observer 1		Observer 2		Observer 3		Pooled Data	
Lesion Group and Imaging Modality	Sensitivity*	PPV†	Sensitivity*	PPV†	Sensitivity*	PPV†	Sensitivity*	PPV†
All lesions (*n* = 179)								
Gadoxetic acid set	81.0 (145)	98.6 (2)	82.1 (147)	98.7 (2)	80.5 (144)	98.0 [3]	81.4 (437)‡	98.4 [7]
DW imaging set	79.9 (143)	96.6 (5)	77.7 (139)	97.2 (4)	78.8 (141)	96.6 [5]	78.8 (423)‡	96.8 [14]
Combined set	92.7 (166)§	98.2 (3)	91.1 (163)§	98.2 (3)	93.3 (167)§	97.1 [5]	92.4 (496)‡	97.8 [11]
Lesions ≤1.0 cm (*n* = 55)								
Gadoxetic acid set	58.2 (32)	94.1 (2)	61.8 (34)	94.4 (2)	56.4 (31)	93.9 [2]	58.8 (97)	94.2 [6]
DW imaging set	63.6 (35)	87.5 (5)	56.4 (31)	88.6 [4]	60.0 (33)	89.2 [4]	60.0 (99)	88.4 [13]
Combined set	85.5 (47)§	94.0 (3)	81.8 (45)§	93.8 [3]	87.3 (48)§	92.3 [4]	84.8 (140)§	93.3 [10]
Lesions >1.0 cm (*n* = 124)								
Gadoxetic acid set	91.13 (113)	100 (0)	91.13 (113)	100 [0]	91.13 (113)	99.1 [1]	91.1 (339)‡	99.7 [1]
DW imaging set	87.1 (108)‖	100 (0)	87.1 (108)‖	100 [0]	87.1 (108)‖	99.1 [1]	87.1 (324)‡	99.7 [1]
Combined set	96.0 (119)‖	100 (0)	95.2 (118)‖	100 [0]	96.0 (119)‖	99.2 [1]	95.7 (356)‡	99.7 [1]

* Numbers in parentheses are the number of true-positive lesions.

† Numbers in parentheses are false-positive lesions. PPV = positive predictive value.

‡ Statistically significant difference ($P < .001$).

§ Values for combined set are significantly higher than those for each set alone ($P = .001$ or $P = .003$).

‖ Statistically significant differences among values ($P = .003$ for observers 1 and 3; $P = .006$ for observer 2).

in specificities among image sets (P = .25–.99) (Tables 4, 5).

False Negatives

There were 11 HCCs that were not verified by any observer on either individual or combined image sets (Table 6). Eight of these HCCs were histologically confirmed at liver transplantation in six patients classified as having Child-Pugh class B or C cirrhosis. A review of these lesions showed that three of them were not seen on the gadoxetic acid set or the DW imaging set. The remaining six were seen as subtle arterially enhanced nodules or as hypointense only on HBP images, and two were subtly hyperintense only on DW images (Fig 3). There were seven lesions that were not verified by any observer on the gadoxetic acid set, but were clearly discerned on the DW image set. In the retrospective review, these lesions were observed as hypointense on HBP images only (n = 5) (Fig 4) or as arterially enhanced nodules without hypointensity on HBP images (n = 2). There were 12 HCCs that were not verified by any observers on the DW image set but were clearly discerned on the gadoxetic acid set. A review of these lesions showed that eight of them,

Table 5

Specificity and Negative Predictive Values for Detection of 144 Benign Lesions

	Observer 1		Observer 2		Observer 3		Pooled Data	
Lesion Group and Image Set	Specificity*	NPV†	Specificity*	NPV†	Specificity*	NPV†	Specificity*	NPV†
All lesions (n = 144)								
Gadoxetic acid set	98.6 (142)	80.7 (34)	98.6 (142)	81.6 (32)	97.9 (141)	80.1 (35)	98.4 (425)	80.8 (101)
DW imaging set	96.5 (139)	79.4 (36)	97.2 (140)	77.8 (40)	96.5 (139)	78.5 (38)	96.8 (418)	78.6 (114)
Combined set	97.9 (141)	91.6 (13)‡	97.9 (141)	89.8 (16)‡	96.5 (139)	92.1 (12)‡	97.5 (421)	91.1 (41)‡
Lesions ≤1.0 cm (n = 61)								
Gadoxetic acid set	96.7 (59)	72.0 (23)	96.7 (59)	73.8 (21)	96.7 (59)	71.1 (24)	96.7 (177)	72.2 (68)
DW imaging set	91.8 (56)	73.7 (20)	93.4 (57)	70.4 (24)	93.4 (57)	72.2 (22)	92.9 (170)	72.0 (66)
Combined set	95.1 (58)	87.9 (8)‡	95.1 (58)	85.3 (10)‡	93.4 (57)	89.1 (7)‡	94.5 (173)	87.4 (25)‡
Lesions >1.0 cm (n = 83)								
Gadoxetic acid set	100.0 (83)	88.3 (11)	100.0 (83)	88.3 (11)	98.8 (82)	88.2 (11)	99.6 (248)	88.6 (32)
DW imaging set	100.0 (83)	83.8 (16)§	100.0 (83)	83.8 (16)§	98.8 (82)	83.7 (16)§	99.6 (248)	83.8 (48)§
Combined set	100.0 (83)	94.3 (5)§	100.0 (83)	93.3 (6)§	98.8 (82)	94.3 (5)§	99.6 (248)	93.9 (16)§

* Numbers in parentheses are number of true-negative lesions.

† Numbers in parentheses are false-negative lesions. NPV = negative predictive value.

‡ Values of combined set are significantly higher than those of each set alone ($P < .001$ or $P = .003$).

§ Differences between values are significant ($P = .006$).

Table 6

Number of False-Negative Lesions According to Confidence Score

Observer	Confidence Score	Gadoxetic Acid Set	DW Imaging Set	Combined Set
1	0	11 (7)	21 (10)	6
	1 or 2	23 (8)	15 (6)	7
2	0	13 (3)	26 (15)	8
	1 or 2	19 (6)	14 (1)	8
3	0	13 (5)	20 (12)	6
	1 or 2	22 (8)	18 (4)	6

Note.—Data in parentheses are number of false-negative lesions that were found to be positive during review of the other set or the combined set.

found in patients who were classified as having Child-Pugh class B or C cirrhosis, were not discerned even at retrospective review (Fig 5). For each observer, seven to nine HCCs were not verified on the individual sets, but were clearly discerned on the combined set. For all HCCs and HCCs 1 cm or smaller, the combined set yielded significantly higher negative predictive values than did each image set individually ($P < .001$ or $P = .003$).

False Positives

For the positive predictive values, the three sets of images showed similar values for all observers (Table 2). Overall, there was only one false-positive lesion that was misclassified as HCC (category 3 or 4) by the observers. This lesion was confirmed to be a hyalinized hemangioma at surgical resection. For each observer, additional false-positive lesions (n = 2–5) were diagnosed on each image set or the combined set. These lesions proved to be dysplastic nodules (n = 3) (Fig 6) or eosinophilic necrosis (n = 2). Three dysplastic nodules were seen as hypointense on HBP images and hyperintense on DW images. The remaining dysplastic nodules (n = 24) or large regenerative nodules (n = 3) assigned to categories 1 or 2 were hypointense on HBP images but were not hyperintense on DW images.

Interobserver Agreement

The κ values for the three observers were 0.709–0.873 for the gadoxetic acid set, 0.782–0.905 for the DW set, and 0.753–0.926 for the combined set, thus indicating good or excellent interobserver agreement with regard to the presence of lesions (Table E1 [online]).

Discussion

Our study results demonstrated that the sensitivities of the combined set were significantly higher than those of each set of images alone. Thus, our results are in general accordance with the previous data of Piana et al (20), who showed that combining the hyperintensity on DW images with the conventional HCC criteria on gadolinium-enhanced images yielded an increase in sensitivity for the diagnosis of HCCs smaller than 2 cm. The most noticeable finding in our study is that a considerable number of false-negative lesions were identified that did not fulfill the diagnostic criteria. Seven false-negative lesions that all the observers misclassified on the basis of the gadoxetic acid set were discerned on the DW image set. These lesions were not missed, but the diagnoses were assigned a low confidence level on the basis of the gadoxetic acid

set, because they showed only arterial enhancement or hypointense nodules on HBP images. Furthermore, given the importance of the HBP image in detection of small hypovascular HCCs, a considerable number of small HCCs were easily overlooked in the HBP set, particularly lesions located adjacent to the vessels. Thus, hyperintensity on DW images could contribute to improving the detection of small HCCs by helping to reduce the number of mischaracterized lesions and by allowing more accurate characterization of equivocal lesions.

Because HCCs are less cellular and the tissue structures are analogous to the cirrhotic parenchyma, they may not be reliably detected with DW imaging, compared with metastases (14,21,22). Furthermore, the cirrhotic liver can show restricted diffusion, which makes it difficult to identify HCC in a severely cirrhotic liver, compared with a noncirrhotic or mildly cirrhotic liver (23,24). Of the 13 HCCs that the observers did not diagnose on the basis of the DW images, eight were in patients with Child-Pugh class B or C cirrhosis. DW imaging also has inherent limitations, including limited spatial resolution; susceptibility to motion artifacts, especially for lesions located in the left lateral segment and close to the diaphragm because of cardiac motion; and difficulty in differentiation of solid hepatic masses (11,14,25). Therefore, DW imaging is not generally used alone in clinical scenarios. Since DW imaging is easy to perform and DW images acquired after administration of gadoxetic acid are reportedly comparable to unenhanced DW images (26), a shortened protocol can be adopted by introducing DW imaging during the dynamic phase and the HBP. Thus, the inherent shortcomings of each technique could be counterbalanced by those of the other technique to improve the diagnosis of small HCCs in the combined set.

With currently available imaging criteria for HCC such as the Association for the Study of Liver Diseases criteria (27,28), the diagnosis of malignancy applies only for nodules that are larger than 1 cm and show typical vascular profiles, which ensures a 100% specificity rather than high sensitivity. Therefore, diagnoses of HCCs smaller than 1 cm or that show an atypical vascular pattern are still made on the basis of positive biopsy results, or patients with those lesions are recommended for follow-up examination. This emphasizes the need to refine new diagnostic parameters for HCC and to include state-of-the-art imaging in addition to conventional dynamic imaging techniques that focus only on tumor vascular patterns. In our study, the combined image set made it possible to reliably diagnose hypovascular HCCs or HCCs smaller than 1.0 cm. Despite the small tumor size, good or excellent interobserver agreement was demonstrated for the combined set of images. Thus, our results offer reproducible data. However, three high-grade dysplastic nodules and five hypovascular HCCs were seen as hypointense on HBP images and hyperintense on DW images. Because the first priority of imaging criteria for HCC is to achieve 100% specificity, introducing DW images into the HCC criteria might be debatable. Particularly in patients who are candidates for liver transplantation, the slightly lower specificity of the combined set compared with the gadoxetic acid set for HCCs smaller than 1 cm—although not significantly different for any of the observers—might raise a problem of false-positive HCC detection. Nevertheless, two HCCs were seen only on DW images but not on images obtained with other sequences, and seven to nine lesions diagnosed as HCC that were assigned low confidence levels at review of the individual image sets were verified to be HCC at review of the combined set. In some institutions, high-grade dysplastic nodules are considered to be premalignant lesions and are subject to treatment (29). In these cases, the combined image set might lead to the diagnosis of both HCC and high-risk nodules. Our study results left some areas of uncertainty, particularly concerning the interpretation of hypovascular hypointense nodules that show hyperintensity on DW images or nodules depicted only on DW

Figure 3

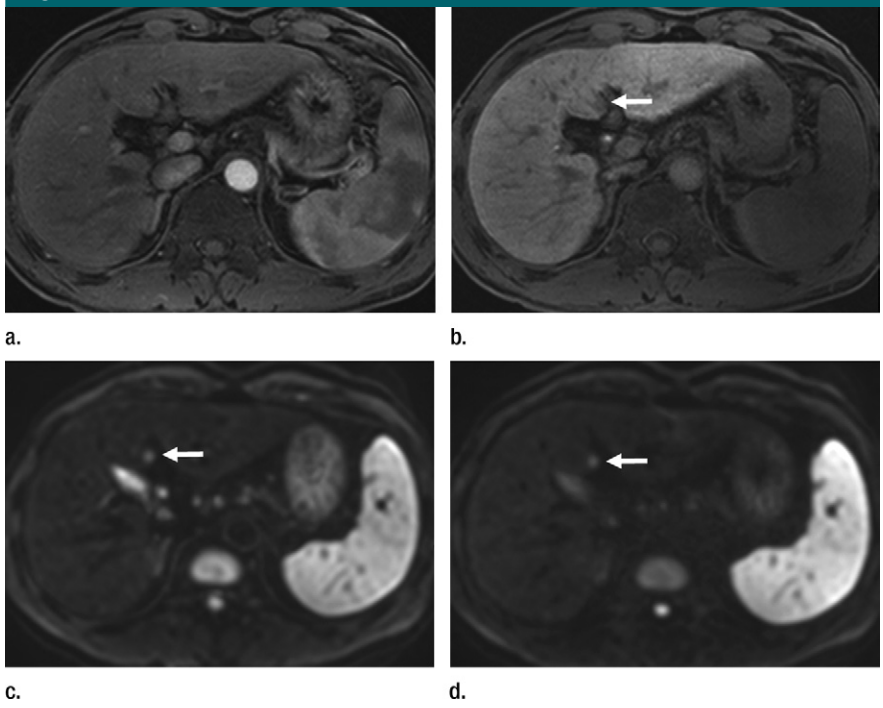

Figure 3: HCC in a 66-year-old man. On axial **(a)** arterial phase image and **(b)** HBP MR image obtained 20 minutes after administration of gadoxetic acid, subtle hypointensity on **b** (arrow) is suggestive of HCC but is not definitive. On axial single-shot echo-planar diffusion weighed images at **(c)** $b = 100$ sec/mm^2 and **(d)** $b = 800$ sec/mm^2, small nodule shows hyperintensity (arrow) but was either missed or diagnosed as HCC with low confidence levels by all observers during image interpretation.

Figure 4

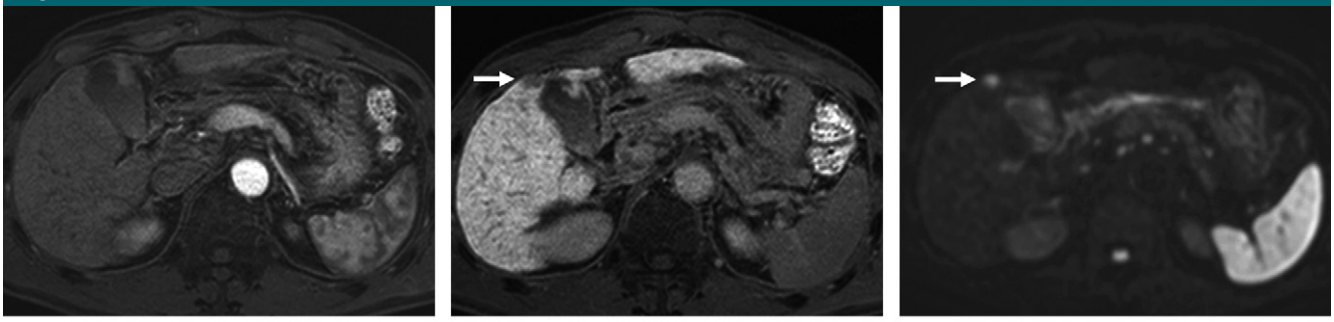

a. b. c.

Figure 4: HCC in a 66-year-old man. On axial **(a)** arterial phase image and **(b)** HBP image obtained 20 minutes after administration of gadoxetic acid, tumor is hypointense only on **b** (arrow) with no arterial hypervascularization. Observers diagnosed as HCC with confidence level of 1. **(c)** On axial single-shot echo-planar DW image at $b = 800$ sec/mm^2, tumor is clearly hyperintense (arrow).

Figure 5

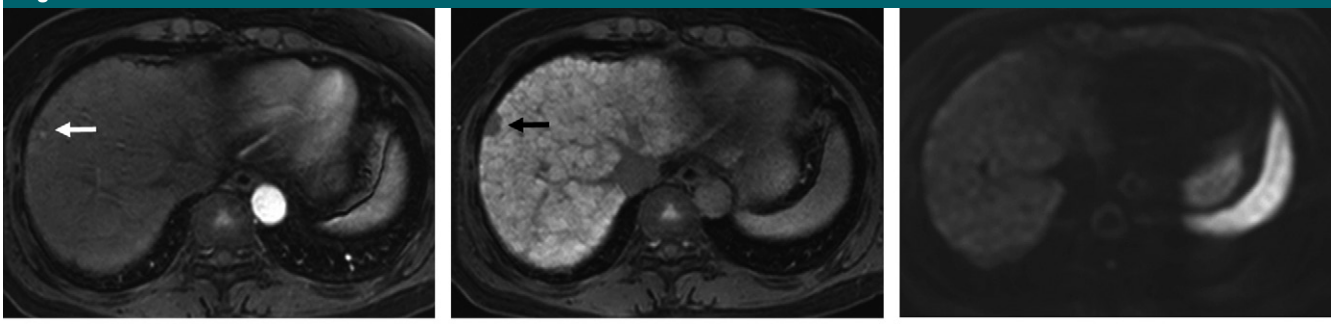

a. b. c.

Figure 5: HCC in a 55-year-old man with Child-Pugh class B cirrhosis. On axial **(a)** arterial phase image and **(b)** HBP image obtained 20 minutes after administration of gadoxetic acid, small HCC shows faint arterial hypervascularization on **a** and hypointensity (arrow) on **b**. **(c)** On axial single-shot echo-planar DW image at $b = 800$ sec/mm^2, tumor is not clearly seen.

Figure 6

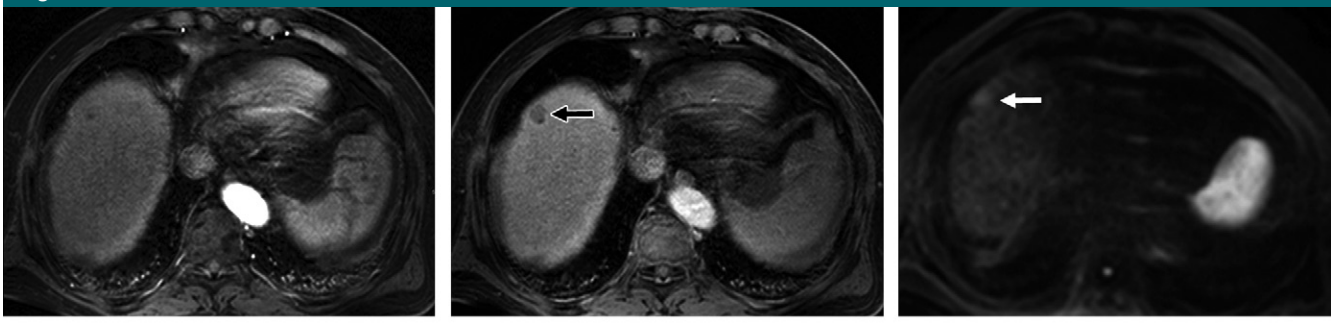

a. b. c.

Figure 6: Dysplastic nodule in a 57-year-old man. On axial **(a)** arterial phase image and **(b)** HBP image obtained 20 minutes after administration of gadoxetic acid, small nodule shows hypointensity with no arterial hypervascularization (arrow). **(c)** On axial single-shot echo-planar DW image at $b = 800$ sec/mm^2, nodule (arrow) is hyperintense. All observers diagnosed lesion as HCC with confidence level 3.

images. These issues are open to further investigation.

Our study had limitations. First, our study included only patients suspected of having small HCCs on the basis of multidetector CT findings obtained during routine HCC workup, which might have caused selection bias. Second, limited numbers of lesions were diagnosed at liver transplantation, which might have resulted in overestimation of the diagnostic performance of MR imaging by

decreasing the number of false-negative lesions. Furthermore, owing to inconsistencies in the reference standard, we did not include all cirrhosis-associated benign hepatocellular nodules that were pathologically proved but not verified at imaging. Third, although we used ROC analysis for detection of HCC, detailed imaging criteria for benign lesions were not established when scoring was performed. This might be the cause of some false-positive results. However, as in real clinical practice, most of benign lesions with typical imaging features were differentiated from HCCs through interpretation of unenhanced images, contrast-enhanced images, and DW images.

In conclusion, the combination of gadoxetic acid–enhanced MR imaging and DW imaging yielded better diagnostic accuracy and sensitivity in the detection of small HCCs than did either technique of imaging alone, because it helped to reduce the likelihood of overlooked lesions and to increase reader confidence in evaluating equivocal hepatocellular nodules.

Disclosures of Potential Conflicts of Interest: M.J.P. No potential conflicts of interest to disclose. **Y.K.K** No potential conflicts of interest to disclose. **M.W.L.** No potential conflicts of interest to disclose. **W.J.L.** No potential conflicts of interest to disclose. **Y.S.K.** No potential conflicts of interest to disclose. **S.H.K.** No potential conflicts of interest to disclose. **D.C.** No potential conflicts of interest to disclose. **H.R.** No potential conflicts of interest to disclose.

References

1. Parkin DM, Bray F, Ferlay J, Pisani P. Estimating the world cancer burden: Globocan 2000. Int J Cancer 2001;94(2):153–156.
2. Yeh CN, Chen MF, Lee WC, Jeng LB. Prognostic factors of hepatic resection for hepatocellular carcinoma with cirrhosis: univariate and multivariate analysis. J Surg Oncol 2002;81(4):195–202.
3. Adler M, De Pauw F, Vereerstraeten P, et al. Outcome of patients with hepatocellular carcinoma listed for liver transplantation within the Eurotransplant allocation system. Liver Transpl 2008;14(4):526–533.
4. Yuen MF, Cheng CC, Lauder IJ, Lam SK, Ooi CG, Lai CL. Early detection of hepatocellular carcinoma increases the chance of treatment: Hong Kong experience. Hepatology 2000;31(2):330–335.
5. Bruix J, Llovet JM. Major achievements in hepatocellular carcinoma. Lancet 2009; 373(9664):614–616.
6. Park G, Kim YK, Kim CS, Yu HC, Hwang SB. Diagnostic efficacy of gadoxetic acid-enhanced MRI in the detection of hepatocellular carcinomas: comparison with gadopentetate dimeglumine. Br J Radiol 2010;83(996):1010–1016.
7. Kim YK, Kim CS, Han YM, Park G. Detection of small hepatocellular carcinoma: can gadoxetic acid-enhanced magnetic resonance imaging replace combining gadopentetate dimeglumine-enhanced and superparamagnetic iron oxide-enhanced magnetic resonance imaging? Invest Radiol 2010;45(11):740–746.
8. Yoon SH, Lee JM, So YH, et al. Multiphasic MDCT enhancement pattern of hepatocellular carcinoma smaller than 3 cm in diameter: tumor size and cellular differentiation. AJR Am J Roentgenol 2009;193(6): W482–W489.
9. Park MJ, Kim YS, Lee WJ, Lim HK, Rhim H, Lee J. Outcomes of follow-up CT for small (5-10-mm) arterially enhancing nodules in the liver and risk factors for developing hepatocellular carcinoma in a surveillance population. Eur Radiol 2010;20(10):2397–2404.
10. Forner A, Vilana R, Ayuso C, et al. Diagnosis of hepatic nodules 20 mm or smaller in cirrhosis: Prospective validation of the noninvasive diagnostic criteria for hepatocellular carcinoma. Hepatology 2008;47(1):97–104.
11. Nasu K, Kuroki Y, Tsukamoto T, Nakajima H, Mori K, Minami M. Diffusion-weighted imaging of surgically resected hepatocellular carcinoma: imaging characteristics and relationship among signal intensity, apparent diffusion coefficient, and histopathologic grade. AJR Am J Roentgenol 2009;193(2):438–444.
12. Parikh T, Drew SJ, Lee VS, et al. Focal liver lesion detection and characterization with diffusion-weighted MR imaging: comparison with standard breath-hold T2-weighted imaging. Radiology 2008;246(3):812–822.
13. Taouli B, Koh DM. Diffusion-weighted MR imaging of the liver. Radiology 2010;254(1): 47–66.
14. Kim YK, Kim CS, Han YM, Lee YH. Detection of liver malignancy with gadoxetic acid-enhanced MRI: is addition of diffusion-weighted MRI beneficial? Clin Radiol 2011;66(6):489–496.
15. Kim JE, Kim SH, Lee SJ, Rhim H. Hypervascular hepatocellular carcinoma 1 cm or smaller in patients with chronic liver disease: characterization with gadoxetic acid-enhanced MRI that includes diffusion-weighted imaging. AJR Am J Roentgenol 2011;196(6):W758–W765.
16. Obuchowski NA, McClish DK. Sample size determination for diagnostic accuracy studies involving binormal ROC curve indices. Stat Med 1997;16(13):1529–1542.
17. Chakraborty DP, Winter LH. Free-response methodology: alternate analysis and a new observer-performance experiment. Radiology 1990;174(3 Pt 1):873–881.
18. Obuchowski NA. Nonparametric analysis of clustered ROC curve data. Biometrics 1997;53(2):567–578.
19. Landis JR, Koch GG. The measurement of observer agreement for categorical data. Biometrics 1977;33(1):159–174.
20. Piana G, Trinquart L, Meskine N, Barrau V, Beers BV, Vilgrain V. New MR imaging criteria with a diffusion-weighted sequence for the diagnosis of hepatocellular carcinoma in chronic liver diseases. J Hepatol 2011;55(1):126–132.
21. Bruegel M, Holzapfel K, Gaa J, et al. Characterization of focal liver lesions by ADC measurements using a respiratory triggered diffusion-weighted single-shot echoplanar MR imaging technique. Eur Radiol 2008;18(3):477–485.
22. Kanematsu M, Hoshi H, Murakami T, et al. Fat-suppressed T2-weighted MR imaging of hepatocellular carcinoma and metastases: comparison of conventional spin-echo, fast spin-echo, and echoplanar pulse sequences. J Magn Reson Imaging 1999;10(1):25–32.
23. Taouli B, Tolia AJ, Losada M, et al. Diffusion-weighted MRI for quantification of liver fibrosis: preliminary experience. AJR Am J Roentgenol 2007;189(4):799–806.
24. Luciani A, Vignaud A, Cavet M, et al. Liver cirrhosis: intravoxel incoherent motion MR imaging—pilot study. Radiology 2008;249(3):891–899.
25. Vandecaveye V, De Keyzer F, Verslype C, et al. Diffusion-weighted MRI provides additional value to conventional dynamic contrast-enhanced MRI for detection of hepatocellular carcinoma. Eur Radiol 2009; 19(10):2456–2466.
26. Choi JS, Kim MJ, Choi JY, Park MS, Lim JS, Kim KW. Diffusion-weighted MR imaging of liver on 3.0-Tesla system: effect of intravenous administration of gadoxetic acid disodium. Eur Radiol 2010;20(5):1052–1060.
27. Bruix J, Sherman M; American Association for the Study of Liver Diseases. Management of hepatocellular carcinoma: an update. Hepatology 2011;53(3):1020–1022.
28. Bruix J, Sherman M, Llovet JM, et al. Clinical management of hepatocellular carcinoma. Conclusions of the Barcelona-2000 EASL conference. European Association for the Study of the Liver. J Hepatol 2001;35(3):421–430.
29. Bolondi L, Gaiani S, Celli N, et al. Characterization of small nodules in cirrhosis by assessment of vascularity: the problem of hypovascular hepatocellular carcinoma. Hepatology 2005;42(1):27–34.